AMERICAN SOCIETY FOR MICROBIOLOGY | Journal of Bacteriology®

RESEARCH ARTICLE

Distinct Domains of CheA Confer Unique Functions in Chemotaxis and Cell Length in *Azospirillum brasilense* Sp7

Jessica M. Gullett, Amber Bible,* Gladys Alexandre

Department of Biochemistry and Cellular and Molecular Biology, University of Tennessee, Knoxville, Tennessee, USA

ABSTRACT Chemotaxis is the movement of cells in response to gradients of diverse chemical cues. Motile bacteria utilize a conserved chemotaxis signal transduction system to bias their motility and navigate through a gradient. A central regulator of chemotaxis is the histidine kinase CheA. This cytoplasmic protein interacts with membrane-bound receptors, which assemble into large polar arrays, to propagate the signal. In the alphaproteobacterium *Azospirillum brasilense*, Che1 controls transient increases in swimming speed during chemotaxis, but it also biases the cell length at division. However, the exact underlying molecular mechanisms for Che1-dependent control of multiple cellular behaviors are not known. Here, we identify specific domains of the CheA1 histidine kinase implicated in modulating each of these functions. We show that CheA1 is produced in two isoforms: a membrane-anchored isoform produced as a fusion with a conserved seven-transmembrane domain of unknown function (TMX) at the N terminus and a soluble isoform similar to prototypical CheA. Site-directed and deletion mutagenesis combined with behavioral assays confirm the role of CheA1 in chemotaxis and implicate the TMX domain in mediating changes in cell length. Fluorescence microscopy further reveals that the membrane-anchored isoform is distributed around the cell surface while the soluble isoform localizes at the cell poles. Together, the data provide a mechanism for the role of Che1 in controlling multiple unrelated cellular behaviors via acquisition of a new domain in CheA1 and production of distinct functional isoforms.

IMPORTANCE Chemotaxis provides a significant competitive advantage to bacteria in the environment, and this function has been transferred laterally multiple times, with evidence of functional divergence in different genomic contexts. The molecular principles that underlie functional diversification of chemotaxis in various genomic contexts are unknown. Here, we provide a molecular mechanism by which a single CheA protein controls two unrelated functions: chemotaxis and cell length. Acquisition of this multifunctionality is seemingly a recent evolutionary event. The findings illustrate a mechanism by which chemotaxis function may be co-opted to regulate additional cellular functions.

KEYWORDS *Azospirillum*, chemotaxis, signal transduction

Chemotaxis, the directed movement of motile bacteria in gradients of diverse chemoeffectors, promotes colonization of various niches and the establishment of plant-microbe associations (1, 2). The histidine kinase CheA is a central regulator of chemotaxis. In the *Escherichia coli* model, when chemical signals bind to chemoreceptors, CheA is autophosphorylated. This phospho-CheA then promotes changes in swimming direction via phosphotransfer to CheY, yielding phospho-CheY with an increased affinity to flagellar motors. A chemotaxis-specific phosphatase, CheZ, acts on phospho-CheY to terminate the signal. Phospho-CheA also plays a role in receptor

Received 14 March 2017 **Accepted** 11 April 2017

Accepted manuscript posted online 17 April 2017

Citation Gullett JM, Bible A, Alexandre G. 2017. Distinct domains of CheA confer unique functions in chemotaxis and cell length in *Azospirillum brasilense* Sp7. J Bacteriol 199:e00189-17. https://doi.org/10.1128/JB.00189-17.

Editor Ann M. Stock, Rutgers University-Robert Wood Johnson Medical School

Address correspondence to Gladys Alexandre, galexan2@utk.edu.

* Present address: Amber Bible, Biosciences Division, Oak Ridge National Laboratory, Oak Ridge, Tennessee, USA.

All authors contributed equally to this article.

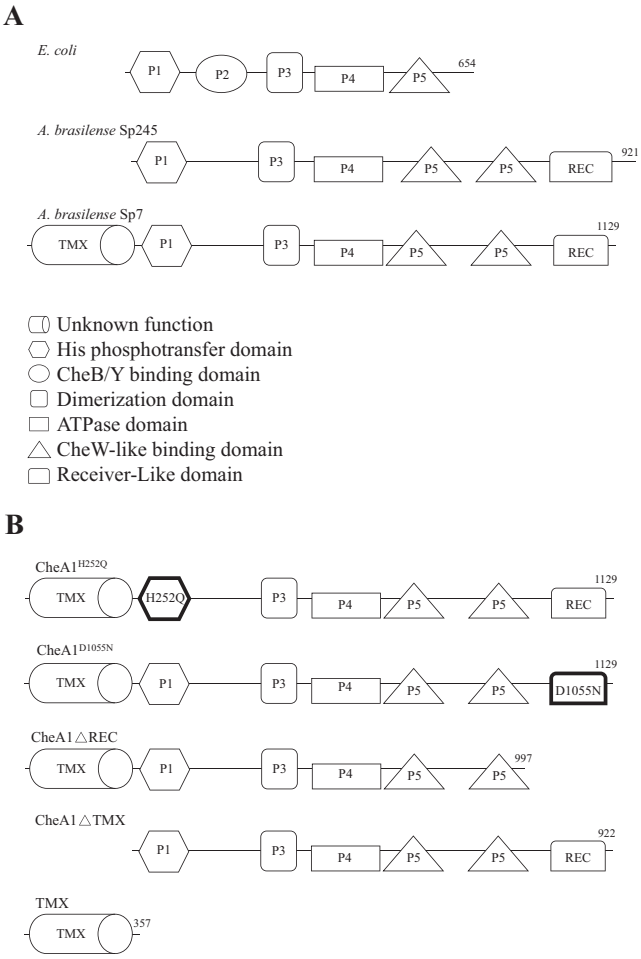

FIG 1 (A) Domain architecture of CheA orthologs in *E. coli* and *A. brasilense* strains Sp7 and Sp245. Top, the *E. coli* CheA contains a histidine phosphotransfer domain which harbors the conserved His residue (P1) followed by a CheB/Y binding domain (P2). The dimerization (dimer) domain (P3) precedes the ATPase domain (P4), which is necessary to phosphorylate the His residue. The binding domain (P5) resides in the C-terminal region. Middle, *A. brasilense* strain Sp245 CheA1 possesses the P1, P3, P4, and P5 domains and also a receiver-like (REC) domain. Bottom, *A. brasilense* strain Sp7 CheA1 possesses domains similar to those of strain Sp245, but it also possesses an N-terminal seven-transmembrane region of unknown function (TMX). Numbers at the C termini denote the total number of amino acids present. (B) Schematic representation of *A. brasilense* strain Sp7 CheA1 variants used in this study. Variants with single-residue replacements (CheA1^{H252Q} and CheA1^{D1055N}) are in boldface.

adaptation to background conditions. Methylation levels of the chemoreceptors are altered through either a phosphotransfer from phospho-CheA to the methylesterase CheB or by the addition of methyl groups via the methyltransferase CheR (3, 4). *E. coli* possesses a single chemotaxis system, and the functional CheA is a homodimer, with each monomer containing five domains denoted P1 to P5 (Fig. 1A) (5). The ATP binding domain of CheA (P4) phosphorylates at the conserved histidine residue in the N-terminal phosphorylation domain (P1) (Fig. 1A). P2 is a docking site for interactions with CheY and CheB, which are both activated through a phosphorylation event from phospho-CheA; P3 serves as a dimerization domain. The P5 domain closely resembles and also interacts with the adaptor protein CheW, which couples chemoreceptors to CheA (6). Together, CheA, through its P5 domains, and CheW interact with the cytoplasmic tips of the trimers of receptor dimers to form a ring-shaped baseplate (7, 8). Each baseplate interacts with neighboring baseplates, making chemotaxis signal transduction a cooperative process that both amplifies and propagates the chemotaxis signal (7–9).

Compared to the case for *E. coli* chemotaxis, the complete genome sequences of most motile bacteria indicate the presence of more than one chemotaxis (Che) operon.

In addition to chemotaxis, some chemotaxis systems are implicated in the regulation of cellular functions other than flagellar motility: some systems regulate the extension-retraction cycle of type IV pili to promote twitching (10), others regulate enzymatic activities implicated in the transition from a vegetative to a sessile lifestyle (11), and some exert control of developmental programs (12–14). Chemotaxis systems that regulate alternative cellular functions often lack a CheY homolog and instead possess enzymes or transcription factors that function to mediate the signaling output (15). Chemotaxis systems that control type IV pili activities are characterized by CheA homologs which possess multiple P1 domains at their N terminus (15). Therefore, comparative analysis of the architecture of chemotaxis systems can provide clues as to the putative function of some chemotaxis operons.

The alphaproteobacterium *Azospirillum brasilense*'s genome encodes four signal transduction pathways. The Che1 pathway controls transient changes in the swimming speed that accompany the simultaneous suppression of changes in the swimming direction during a response to a chemoattractant (16). These changes in swimming velocity modulate the propensity of cells to clump by cell-cell interactions (16–18). However, deletion of *che1* or of the gene for the histidine kinase of the Che1 pathway, *cheA1*, has a minor effect on chemotaxis (17). An additional Che pathway, which has a more dominant role in controlling chemotaxis, has recently been identified (19). In addition to regulating transient increases in swimming speed, Che1 is implicated in regulating cell length: mutations that render *cheA1*, *che1*, or *cheY1* nonfunctional also result in cells of relatively shorter lengths than the wild type, while mutations that abolish the function of enzymes required for chemotaxis receptor adaptation, CheB1 and CheR1, result in cells significantly longer than the wild type, with these effects most evident in dividing cells (17). These data thus suggest that Che1 regulates two distinct functions, i.e., transient changes in swimming speed upon chemo-stimulation and cell length, but the underlying mechanisms are not known (16). The *A. brasilense* Che1 pathway comprises all homologs of the *E. coli* chemotaxis operon, including a CheY1 homolog that functions to regulate transient increases in swimming velocity but excluding CheZ (16). Che1 also includes a CheA1 homolog with an additional N-terminal domain of unknown function (20). In this study, we aimed to identify the domain(s) of CheA1 that contributes to these distinct functions, namely, chemotaxis and cell length regulation. We provide experimental evidence that the N-terminal domain of CheA1, which we name TMX, is dispensable for chemotaxis but is associated with the function of CheA1 in cell length regulation. We also show that CheA1 is produced in two isoforms: (i) a soluble isoform lacking the N-terminal TMX which localizes as small foci at the cell poles and (ii) a larger, membrane-anchored, full-length protein that is distributed throughout the cell surface. Together, our data suggest a molecular mechanism by which the *A. brasilense* Che1 pathway regulates unrelated cellular functions via the production of functionally and spatially distinct populations of CheA1.

RESULTS

Domain architecture reveals unique N-terminal fusion to CheA1. To determine how CheA1 from *A. brasilense* may regulate multiple cellular functions, we first analyzed its domain architecture. Compared to the canonical *E. coli* CheA, the *A. brasilense* CheA1 lacks a P2 domain, contains a second P5 domain, and carries a receiver (REC) domain at the C terminus (SM00448) (Fig. 1A) (21). Strikingly, the *A. brasilense* strain Sp7 CheA1 also possesses an additional N-terminal domain, which we refer to here as TMX, predicted to be closely related to a polytopic hemolysin III-related (HlyIII) protein of unknown function (Fig. 1A). This particular CheA domain appears to be unique to strain Sp7; the CheA1 homolog from the closely related *A. brasilense* strain Sp245 lacks the N-terminal TMX domain but is otherwise similar to the CheA1 of strain Sp7 (Fig. 1A). TMX found at the N terminus of CheA1 from *A. brasilense* Sp7 is thus a unique feature of this protein in this particular strain.

The presence of the N-terminal TMX domain is associated with the CheA1-dependent cell length phenotype but is dispensable for chemotaxis. The different

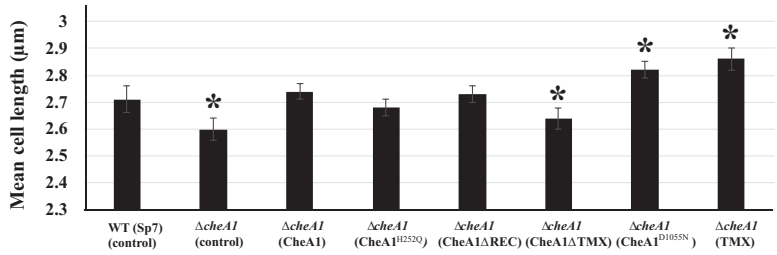

FIG 2 Roles of different domains of CheA1 in cell length regulation. *, statistically significant difference in average cell lengths relative to that of the wild-type strain, at a *P* value of <0.05 ($n = 50$) by Student's *t* test.

architectures of CheA1 in two closely related strains of *A. brasilense* prompted us to repeat the behavioral studies performed in strain Sp7 on strain Sp245. We constructed a derivative of strain Sp245 lacking the CheA1 homolog (Δ*cheA1*$_{Sp245}$) and analyzed chemotaxis and cell length phenotypes. We found that the Δ*cheA1*$_{Sp245}$ mutant was defective in chemotaxis: the average swarm diameter on a soft agar plate was 4.1 $\pm$ 0.03 mm for the wild type and 1.8 $\pm$ 0.02 mm for the Δ*cheA1*$_{Sp245}$ mutant. We also observed that the doubling times of Sp245 and the Δ*cheA1*$_{Sp245}$ mutant were different (6.7 $\pm$ 0.9 h for the wild type and 8.1 $\pm$ 0.8 h for the Δ*cheA1*$_{Sp245}$ mutant), suggesting that the difference in the chemotaxis ring diameter is likely the result of differences in doubling times, since growth is required to observe chemotaxis in this assay. To further evaluate potential chemotaxis defects, we analyzed the swimming pattern of free-swimming cells and found that the Δ*cheA1*$_{Sp245}$ mutant strain was able to reverse swimming direction at a rate similar to that for its parent (data not shown). This suggests that the CheA1 of strain Sp245 is not the major CheA homolog regulating all chemotaxis responses, which is similar to the CheA1 in strain Sp7 (17). Interestingly, mutating *cheA1*$_{Sp245}$ had no effect on cell length: the average length of cells in a population of the wild-type strain Sp245 and its Δ*cheA1*$_{Sp245}$ mutant was 2.6 $\pm$ 0.3 μm. Therefore, the phenotype of the Δ*cheA1*$_{Sp245}$ strain is similar to that of its Sp7 counterpart in that it has no major role in chemotaxis. However, it is distinct from the Sp7 Δ*cheA1* phenotype in that mutating *cheA1* in strain Sp245 does not cause a defect in cell length. These observations suggest that the CheA1-dependent cell length phenotype observed in strain Sp7 is linked to the presence of the TMX domain.

To further characterize the roles of TMX and other CheA1 domains in the control of cell length and chemotaxis, we generated *cheA1* mutants carrying either site-specific mutations of conserved residues or in-frame domain deletions. Specifically, we analyzed CheA1^{H252Q}, a variant with a mutation in the putative autophosphorylation histidine residue previously implicated in CheA1 function during chemotaxis (16), as well as CheA1^{D1055N}, which is mutated in the conserved putative phosphorylatable Asp1055 residue in the C-terminal REC domain of the protein (Fig. 1B). We also constructed and analyzed a strain expressing only the TMX domain, as well as strains expressing CheA1ΔTMX or CheA1ΔREC, which carry in-frame deletions of the TMX domain or the REC domain, respectively (Fig. 1B). As previously described (17), the Δ*cheA1* mutant strain carrying an empty vector produced significantly shorter cells than the Sp7 wild-type strain. However, this defect was complemented by introducing a medium-copy-number plasmid carrying the full-length *cheA1* gene (pBBRCheA1) (Fig. 2). Expressing CheA1^{H252Q} or CheA1ΔREC from a broad-host-range plasmid fully restored cell length to the Δ*cheA1* mutant strain, indicating that CheA1 autophosphorylation and its REC domain play no role in cell length control. In contrast, expressing a CheA1 variant in which TMX was deleted in frame (CheA1ΔTMX) failed to restore the cell length phenotype to the Δ*cheA1* mutant strain (Fig. 2). Surprisingly, expressing CheA1^{D1055N}or TMX alone in the Δ*cheA1* strain not only restored but further increased the cell length (Fig. 2).

The effect of TMX on cell length could possibly result from altered growth rates of the strains carrying these vectors. To address this, doubling times of strains expressing

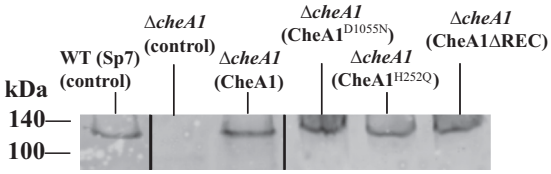

FIG 3 Detection of CheA1 in whole-cell lysates of *A. brasilense* wild-type strain Sp7 and its Δ*cheA1* mutant derivatives expressing CheA1 and its variants from a plasmid by Western blotting. The mutant derivatives were expressing CheA1, variants with single-amino-acid residue replacements, or truncated variants of the protein from a medium-copy-number broad-host-range plasmid. A polyclonal antibody raised against CheA1ΔTMX was affinity purified as described in Materials and Methods prior to use. Each well is identified with the strain and with the parental or variant protein expressed from the broad-host-range vector in parentheses. The black lines indicate junctions separating lanes that were spliced from the original image in order to show samples run on the same gel in a single row.

these CheA1 constructs were determined. The wild-type Sp7(pBBR) (control) strain doubled faster (2.6 ± 0.4 h) than any of the Δ*cheA1* mutant derivatives, but all Δ*cheA1* mutant derivatives had doubling times which were not significantly different from each other. The doubling times were 4.7 ± 0.3 h for the Δ*cheA1*(pBBR) mutant, 5.6 ± 0.5 h for the Δ*cheA1*(pBBRCheA1) mutant, 4.8 ± 0.5 h for the Δ*cheA1*(pBBRCheA1^{H252Q}) mutant, 4.6 ± 0.2 h for the Δ*cheA1*(pBBRCheA1ΔREC) mutant, 4.8 ± 0.5 h for the Δ*cheA1*(pBBRCheA1ΔTMX) mutant, 5.3 ± 0.7 h for the Δ*cheA1*(pBBRCheA1^{D1055N}) mutant, and 4.6 ± 0.2 h for the Δ*cheA1*(pBBRTMX) mutant. These data suggest that the cell length phenotype, which is different in the strains expressing these constructs (Fig. 2), is not directly the result of impaired growth. We also considered the possibility that membrane-bound CheA1 variants could have indirect effects on cell length due to altered protein expression levels from the medium-copy-number plasmid, including protein degradation. To test this, we used a polyclonal antibody raised against soluble CheA1 (CheA1ΔTMX) and Western blots to compare levels of protein expression in the wild type and the Δ*cheA1* mutant strains expressing membrane-bound CheA1 variants (Fig. 3). As expected, the anti-CheA1ΔTMX antibodies recognized a single large band, at the predicted molecular weight, in all strains except the Δ*cheA1* mutant control. Comparing the CheA1 band intensity across the samples revealed that, relative to the wild-type Sp7 strain carrying an empty vector control, the Δ*cheA1* mutant derivatives expressed CheA1 and its variants at levels that were comparable between them and represented about twice the levels of CheA1 detected in the wild type. Specifically, CheA1, CheA1^{H252Q}, CheA1^{D1055N}, and CheA1ΔREC expression levels were on average 1.8, 1.9, 2.0, and 2.2 times the wild-type levels, respectively. Based on these data, we hypothesize that TMX may also be produced at about twice the native levels under these conditions. Despite the observation that the expression of CheA1, or its variants, from the pBBR vector yielded about twice the amount of protein produced under native conditions, we did not see any evidence of degradation. Furthermore, all strains expressed similar CheA1 levels, but they each produced different cell length phenotypes, with expression of CheA1 or CheA1^{H252Q} restoring the wild-type cell length phenotype while expression of CheA1^{D1055N} or CheA1ΔREC caused an increase beyond the wild-type cell length (Fig. 2). These data argue against altered protein expression levels causing the cell length phenotypes and rather suggest that it is the presence of TMX in CheA1 of *A. brasilense* strain Sp7 that is associated with the effect on cell length.

We then assessed TMX's role in chemotaxis through soft agar assays of the wild-type, Δ*cheA1* mutant, and mutant derivatives (Fig. 4A). Chemotaxis was fully restored when CheA1 or CheA1ΔTMX was expressed from the medium-copy-vector in the Δ*cheA1* mutant background (Fig. 4A). However, a plasmid expressing only the TMX domain was unable to restore chemotaxis and, in fact, appeared to inhibit chemotaxis. In *A. brasilense* strain Sp7, CheA1 controls transient increases in free-swimming cell speed in response to attractants, such as oxygen. Therefore, we also analyzed the same CheA1 alleles in a temporal gradient assay for aerotaxis (Fig. 4B). Similar to the response of the wild-type strain carrying an empty vector, expressing CheA1 or CheA1ΔTMX in

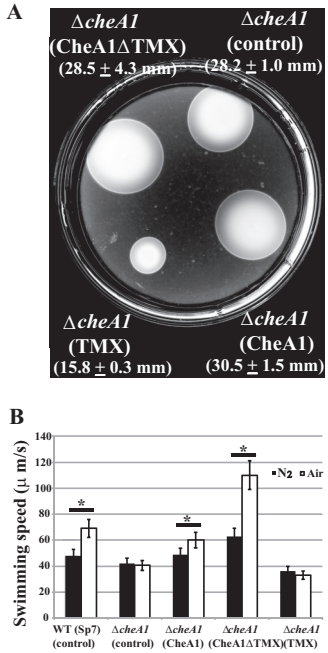

FIG 4 Roles of unique domains of *A. brasilense* strain Sp7 CheA1 in chemotaxis. (A) Chemotaxis of the Δ*cheA1* mutant strain expressing CheA1 or truncated versions of this protein from a broad-host-range plasmid was analyzed in the soft agar plate assay supplemented with appropriate antibiotics. The chemotaxis of the wild-type strain Sp7 carrying an empty vector control [Sp7(pBBR)]; not shown) was similar to that of the Δ*cheA1*(pBBRCheA1) strain, and the average chemotaxis ring diameter was 30.2 ± 2.9 mm. The picture was taken at 48 h postinoculation. The average chemotaxis ring diameters obtained from three replicates are shown. (B) The temporal gradient assay for aerotaxis was used to measure transient increases in cell swimming speed upon switching free-swimming cells from an anaerobic atmosphere (nitrogen gas) to air. Each strain is identified, with the parental or variant protein it expresses from the broad-host-range vector in parentheses. *, statistically significant difference in the swimming speed between before and after switching to air ($P < 0.05$ by Student's *t* test).

the Δ*cheA1* mutant strain resulted in statistically significant increases in the swimming speed in response to a switch from anaerobiosis to air (Fig. 4B). As expected, a Δ*cheA1* mutant strain carrying an empty vector lacked this response. A similar defect was also observed when the TMX domain was expressed alone from a plasmid in this mutant (Fig. 4B). Together, the results suggest that TMX present within CheA1 in *A. brasilense* strain Sp7 is dispensable for chemotaxis.

CheA1 is produced as two isoforms. The results above were puzzling regarding how distinct domains of CheA1 could function in chemotaxis or cell length regulation with no obvious functional overlap. Further, the presence of the predicted polytopic TMX domain at the N terminus of CheA1 suggested that CheA1 from *A. brasilense* may be anchored to the membrane, a proposition which, if confirmed, would challenge existing paradigms regarding the subcellular assembly of chemotaxis signaling complexes, namely, that CheA is a soluble protein which interacts with chemoreceptors at cell poles (3, 22). To address this issue, we analyzed whole-cell extracts of the wild-type strain and the Δ*cheA1* mutant derivative using a Western blot and affinity-purified anti-CheA1 antibodies raised against soluble CheA1 (CheA1ΔTMX). This analysis revealed the presence of two bands present exclusively in the wild-type lysates and absent from the Δ*cheA1* mutant lysates (Fig. 5A). The molecular mass of the full-length CheA1 from strain Sp7 is predicted to be 120 kDa, which we detected as a thick band on whole-cell extracts. In addition, a very faint band that migrated at around 100 kDa was also detected in the whole-cell lysates of the wild-type strain. Similar Western blot analyses of whole-cell lysates of several *Azospirillum* strains, for which the genome is sequenced and not predicted to encode a membrane-anchored CheA1, revealed only one unique cross-reacting band at about 100 kDa (data not shown). Given the specific

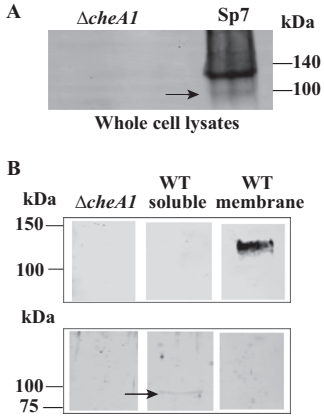

FIG 5 Detection of CheA1 in different subcellular fractions of *A. brasilense* wild-type strain Sp7 and its Δ*cheA1* mutant derivative by Western blotting. (A) Whole-cell lysates of the wild type and the Δ*cheA1* mutant were probed with affinity-purified polyclonal antibodies raised against a recombinantly produced soluble CheA1ΔTMX from *A. brasilense* Sp7, as described in Materials and Methods. (B) Different subcellular fractions collected from the wild-type strain Sp7 were probed with affinity-purified polyclonal antibodies raised against a recombinantly produced soluble CheA1ΔTMX from *A. brasilense* Sp7. Note that different protocols were used for sample preparation and SDS-PAGE for the Western blots shown in panels A and B (see Materials and Methods). In panel A, an anti-CheAΔTMX antibody, which was further purified against whole proteins extracted from the Δ*che1* mutant, was used. These samples were run on a 7.5% gel and transferred to a 0.45-μm hydrophobic PVDF transfer membrane. In panel B, an anti-CheAΔTMX antibody which had not been further purified against whole proteins extracted from the Δ*che1* mutant was used. The membrane fraction was resuspended in a solubilizing buffer (1× PBS with 2% Triton X-100 and 1 mM PMSF) and run on an 8 to 16% gradient gel before being transferred to a nitrocellulose membrane. For the cytosolic fraction, these samples were concentrated via acetone precipitation before being loaded in a 10% gel and transferred to a nitrocellulose membrane. The numbers on the left indicate the positions of the molecular mass markers run on the same gels. The arrows point to the soluble, faint band corresponding to CheA1ΔTMX.

detection of this large band in Sp7 with antibodies raised against the soluble CheA1ΔTMX and the fact that the N-terminal TMX domain is predicted to encode a protein with seven membrane-spanning segments, we hypothesize that the high-molecular-weight band detected in whole-cell lysates of the wild type corresponds to a full-length CheA1 containing the TMX domain and the smaller band corresponds to a soluble CheA1 without the TMX domain. We used cell fractionation to further investigate the subcellular localization of CheA1 (Fig. 5B). A broad band at around 120 kDa, likely corresponding to full-length CheA1, was found exclusively in the membrane fraction of strain Sp7 and was absent in the soluble fraction of this strain or in the lysates of the Δ*cheA1* mutant treated under similar conditions. Analysis of the proteins produced in the soluble fractions of the wild-type strain indicated the presence of a single band corresponding to a product at about 98 kDa that was absent from both the membrane fraction and the Δ*cheA1* lysates (Fig. 5B). The predicted molecular mass of a soluble CheA1 produced without the N-terminal TMX domain is 98 kDa, suggesting the presence of a soluble CheA1 in *A. brasilense* strain Sp7. We note that the samples corresponding to the soluble fraction analyzed here were also more concentrated than the whole-cell lysates or the membrane fraction (Fig. 5), underscoring the low concentration in cells. Based on this observation, we surmise that a soluble CheA1 isoform is present in the cytoplasm of *A. brasilense* at relatively low concentrations compared to the membrane-bound isoform. To determine the relative abundance of bands detected in the Western blots, we used densitometry analysis and found that the thicker band migrating at 120 kDa was about 11-fold more intense than the smaller band. Together, these data indicate that CheA1 from *A. brasilense* strain Sp7 is produced in two isoforms: a membrane-bound form corresponding to a full-length CheA1 anchored to the membrane via the polytopic TMX domain and a soluble form corresponding to CheA1 lacking the TMX domain and that most resembles the architecture of CheA homologs from other organisms.

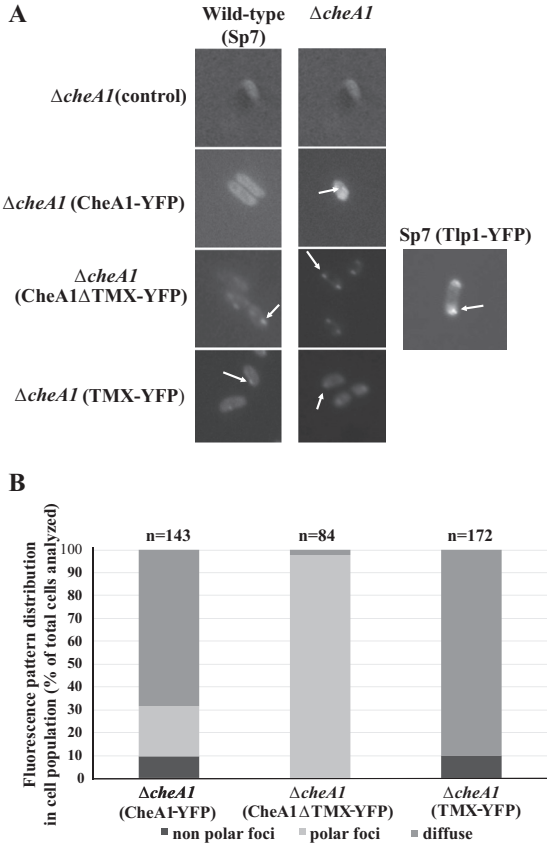

FIG 6 Fluorescence microscopy of YFP-tagged chemotaxis proteins from *A. brasilense* wild-type strain Sp7 and its Δ*cheA1* mutant derivative. (A) Representative fluorescence microscopy images. The fluorescent constructs were expressed from the native *cheA1* promoter on a broad-host-range plasmid, pRH005. For expression of Tlp1-YFP, the fusion was expressed from the *lac* promoter present on the pRH005 vector backbone. Arrows indicate punctate foci in cells. (B) Quantitation of the distribution of fluorescence in the population of cells analyzed. Each strain is identified, with the variant protein fusion to YFP expressed from the broad-host-range vector in parentheses. The total numbers (*n*) of cells analyzed are shown on the graph. The cells included in the analysis were imaged from at least 3 independent cultures.

The CheA1 isoforms localize to the cell surface and to the cell poles. To corroborate the cell fractionation data, we constructed and expressed, from broad-host-range plasmids, fluorescently tagged versions of the full-length CheA1 (CheA1-yellow fluorescent protein [YFP]), of CheA1ΔTMX (CheA1ΔTMX-YFP), and of isolated TMX (TMX-YFP). The fluorescent constructs were expressed in both the wild-type strain Sp7 and the Δ*cheA1* mutant backgrounds (Fig. 6A). The constructs were functional in that they restored the wild-type phenotype in cell length regulation and chemotaxis to a Δ*cheA1* mutant strain (see Fig. S1 in the supplemental material). In both backgrounds, CheA1-YFP was diffuse throughout the cells with occasional foci, both polar and nonpolar, that were relatively dim and seen best when expressed in the Δ*cheA1* strain background. In contrast, CheA1ΔTMX-YFP was present as punctate foci at the cell poles in both strain backgrounds (Fig. 6). The localization of TMX-YFP, expressed in either the Sp7 or Δ*cheA1* strain background, was diffuse throughout the cell, although occasional punctate foci were observed, though they did not appear to localize in any particular region of the cell surface (Fig. 6A). The localization of CheA1ΔTMX-YFP at the cell poles was similar to the localization of a chemotaxis receptor Tlp1-YFP, which was previously shown to function in chemotaxis (23). Quantitative evaluation of the distribution of fluorescence in the cell population expressing CheA1-YFP, CheA1ΔTMX-YFP, and TMX-YFP corroborated these observations (Fig. 6B). In addition, cells expressing CheA1-YFP displayed localization patterns more consistent with those seen in cells expressing TMX-YFP, presumably corresponding to the higher level of membrane-anchored

CheA1-YFP relative to that of the soluble, polar-localized CheA1ΔTMX isoform. Together, these data are consistent with the hypothesis that the soluble isoform of CheA1 localizes as polar clusters while the full-length CheA1 localizes independently to the cell surface via the N-terminal TMX domain.

DISCUSSION

Here we provide experimental evidence supporting a model for the multifunctional role of CheA1 from *A. brasilense* Sp7 in regulating chemotaxis and cell length at division (16, 17). In all *Bacteria* and *Archaea* analyzed to date, the chemotaxis receptors assemble together with cytoplasmic chemotaxis proteins, including CheA homologs, at the cell poles, where they form complex signaling arrays which function to amplify and propagate signals (3, 7, 8, 22). The soluble CheA1 isoform from the Sp7 strain studied here localized at the cell poles, consistent with its function in chemotaxis. The full-length, membrane-anchored CheA1 was distributed throughout the cells, with no apparent distinct localization. Given its localization on the cell surface, the function of the membrane-anchored CheA1, while unknown, is expected to be independent of the chemotaxis signaling function of the protein, consistent with results obtained here. This hypothesis is further supported by the observation that chemotaxis receptor mutants that were shown to signal (e.g., Tlp1 [24] and AerC [25]) and localize at the cell poles (AerC [25]) in a Che1-dependent manner do not display any cell length phenotype, similar to those produced as a result of mutations in *cheA1* (17).

Our results suggest that the N-terminal TMX domain of CheA1 from strain Sp7 plays a role in modulating cell length. Deletion of the sequence corresponding to TMX from CheA1 yielded alleles unable to restore the wild-type cell length phenotype to the Δ*cheA1* mutant, but expression of TMX alone rescued this phenotype. TMX is a conserved, single-domain protein of unknown function that is homologous to a hemolysin III-related (HlyIII) protein in *Bacillus cereus* (26, 27). Some evidence, obtained using recombinantly expressed HlyIII proteins in the heterologous *E. coli* background, suggested that HlyIII-related proteins function as hemolysins (28), but their presence in all bacteria makes this hypothesis unlikely. The function of HlyIII proteins has not been conclusively determined (29), but they were shown to be distant homologs of adipoR receptors found in yeasts and humans (29), the function of which also remains to be established. The data obtained here suggest that TMX, as shown here fused to the *A. brasilense* CheA1 protein, may have a function that ultimately alters how cells control cell length, but a direct role for TMX as a cell length regulator has yet to be established. Whether this is a conserved function of HlyIII-related homologs also remains to be determined.

Interestingly, expression of TMX alone or a mutation replacing the conserved aspartate residue within the CheA1 REC domain (D1055) yielded strains that were even longer than the wild-type strain. This is unexpected, and it also suggests possible features for TMX function. First, the deletion of the REC domain in CheA1ΔREC did not have this effect on the cell length phenotype, suggesting that it is not a direct function of the REC domain. The cell length phenotype of the CheA1^{D1055N} mutant supports our findings that CheA1 is produced as a full-length, membrane-anchored isoform, and it further suggests that phosphorylation of the conserved aspartate residue within the REC domain has a regulatory role in the TMX output. This is consistent with the previously described functions of REC domains as regulatory modules in other hybrid histidine CheA homologs (30, 31). For example, mutating the REC domain of CheA3, which is involved in controlling cyst development in the closely related *Rhodospirillum centenum*, causes a loss of regulation of cyst formation, as those mutant derivatives produce more cysts than wild-type cells do (10, 31). One interpretation of our data in light of these previous findings is that phosphorylation of D1055 causes a conformational change within the full-length, membrane-anchored CheA1, which ultimately alters the ability of TMX to interact with the target protein(s), thereby affecting the cell length phenotype. The effect of expressing TMX alone, from a plasmid, on cell length

is also consistent with interfering with protein-protein interactions that TMX may be engaged in for its function. This hypothesis is also consistent with previous data showing that other mutations within Che1 proteins (e.g., CheY1) that interact with CheA1 also affect cell length bias (17). Interactions of Che1 proteins with CheA1 are expected to depend on canonical CheA1 domains, which are present in both the soluble and the membrane-anchored CheA1 isoforms. Together, the data thus suggest that the function of TMX in regulating cell length in *A. brasilense* Sp7 may depend on interactions with other proteins.

The existence of CheA isoforms in chemotactic bacteria is not a new concept; *E. coli* produces CheA in two isoforms by utilizing a second translational start site (32, 33). What is unique about the CheA1 isoforms in *A. brasilense* strain Sp7 is that each isoform contributes to the regulation of two unrelated cellular functions. How the two CheA1 isoforms in *A. brasilense* are produced remains to be determined. Unlike in *E. coli*, there is no evidence for the presence of a ribosome binding site that would permit initiation of translation of the soluble CheA1 isoform (20, 32). Other possible mechanisms include transcriptional regulation from an alternative promoter as well as posttranscriptional and/or posttranslational processing. Further experimental investigation is required to establish the exact molecular mechanism involved in the production of these two isoforms.

Our data indicate that the insertion of the polytopic TMX domain at the N terminus of CheA1 of *A. brasilense* strain Sp7 is a recent event. None of the other *Azospirillum* species strains sequenced to date shows evidence of a similar domain insertion (34–39). In fact, the draft genome of an Sp7 strain generated by a team of South Korean scientists also lacks the TMX fusion to CheA1 (NCBI BioProject PRJNA293508). *A. brasilense* genomes are organized as 7 replicons: one chromosome and 6 large plasmids named p1 through p6 (34–39). The DNA regions coding for CheA1 and for TMX are both located on the largest plasmid, p1, in all *A. brasilense* strains with available genome sequences, but they are not adjacent and are separated by several kilobases, precluding a simple frameshifting or slippage mutation between adjacent genes. Genome plasticity and extensive genomic rearrangements are evidenced in the *Azospirillum* genomes sequenced to date, including those of several strains of *A. brasilense* (34–38). These include the lack of synteny between replicons of strains from the same species, the abundance and density of insertion sequence IS elements in all genomes, and evidence of plasmid loss or rearrangements and of repeated phage infections. The recent TMX acquisition by CheA1 of strain Sp7 is also supported by the lack of functional divergence between CheA1 proteins of different *A. brasilense* strains. Our results show that the minor role of the soluble CheA1 in *A. brasilense* Sp7 chemotaxis (16) is conserved in strain Sp245, in which the fusion event between TMX and CheA1 has not occurred. Comparative genome analysis of diverse bacteria shows that most domain acquisition events that generate novel multidomain protein architectures occur at the N or C termini of proteins (40). The insertion of TMX at the N terminus of CheA1 from strain Sp7 is consistent with these observations, but the mechanism involved is unknown. Analyses of protein domain fusion or insertion events in completely sequenced genomes of closely related organisms have been previously used to predict protein-protein interactions (41). However, we have no evidence that TMX and CheA1 functionally interact. Our results here show that the domain acquisition event that fused TMX to CheA1 resulted in both protein functions being maintained through the production of two CheA1 isoforms. While we do not know how TMX exerts its effect on cell length, this function is not obviously related to the control of the motility pattern mediated by CheA1. Mechanistic insight into how TMX functions to regulate cell length in *A. brasilense* should provide conclusive experimental evidence regarding a possible functional relationship.

MATERIALS AND METHODS

Strains, media, and chemicals. The bacterial strains used in this study are listed in Table 1. *A. brasilense* strain Sp7 (ATCC 29145) (42) and mutant derivatives were grown at 28°C on minimal medium

TABLE 1 Strains and plasmids used in this study

Strain or plasmid	Genotype or relevant characteristic(s)	Reference or source
Escherichia coli strains		
Top10	Cloning strain	Invitrogen
OMNImax	Cloning strain	Invitrogen
S17-1	*thi endA recA hsdR* RP4-2Tc::Mu-Km::Tn*7*	25
Azospirillum brasilense strains		
Sp7	Parental strain, wild type	ATCC (ATCC 29145)
Sp245	Parental strain, wild type	20
Δ*cheA1* mutant	Δ(*cheA1*)::*gusA*-Km (Km)	17
Δ*che1* mutant	Δ(*cheA1-cheR1*)::Cm (Cm)	17
$\Delta cheA1_{Sp245}$ mutant	Δ*cheA1*:Gm insertion in Sp245	This work
Plasmids		
pDONR 221	Cloning vector	Invitrogen
Topo 2.1	Cloning vector	Thermo Fisher
pBBR1MCS3	Cloning vector	23
pBSKII(+)	Cloning vector	Stratagene
pRH005	Gateway destination vector for C-terminal YFP fusion with protein of interest	27
pDONRTMX	pDONR221 carrying TMX	This work
pDONRCheA1	pDONR221 carrying CheA1	This work
pDONRCheA1ΔTMX	pDONR221 carrying CheA1ΔTMX	This work
pDONRTlp1	pDONR221 carrying Tlp1	This work
pBBRCheA1	pBBR1MCS3 expressing CheA1	17
pBBRCheA1ΔTMX	pBBR1MCS3 expressing CheA1 with the TMX domain deleted	This work
pBBRCheA1ΔREC	pBBR1MCS3 expressing CheA1 with the REC domain deleted	This work
pBBRTMX	pBBR1MCS3 expressing the TMX domain of CheA1	This work
pRHCheA1	pRH005 expressing CheA1	This work
pRHTMX	pRH005 expressing TMX domain	This work
pRHCheA1ΔTMX	pRH005 expressing CheA1 with the TMX domain deleted	This work
pRHTlp1	pRH005 expressing Tlp1	This work
pKGmob-Gm	Mobilizable suicide plasmid	Lab strain
pKGmob-cheA1	pKGmob-Gm expressing Sp245 CheA1	This work
$pBBRCheA1^{H252Q}$	pBBR1MCS3 expressing $CheA1^{H252Q}$	Lab strain
$pBBRCheA1^{D1055N}$	pBBR1MCS3 expressing $CheA1^{D1055N}$	This work
pBSKCheA1	pBSKII(+) carrying CheA1	This work
pBSKCheA1ΔTMX	pBSKII(+) carrying CheA1 with the TMX domain deleted	This work

for *A. brasilense* (MMAB) plates supplemented with malate (10 mM final concentration) or with both malate (5 mM) and fructose (5 mM) for cell size measurements (see below), since these were determined to be the best substrates to observe cell size differences (43). MMAB is either supplemented with a nitrogen source (ammonium chloride at 18.7 mM), with cells incubated with shaking (200 rpm), or without nitrogen supplementation for growth under nitrogen fixation conditions, without shaking to limit oxygen diffusion. The Δ*cheA1* and $cheA1^{H252Q}$ derivatives were described previously (16, 17) (Table 1).

Behavioral assays. For comparison of chemotaxis responses in the soft agar assay, bacteria were inoculated into MMAB solidified with 0.3% (wt/vol) agar (soft agar plates) and supplemented with 18.7 mM ammonium chloride and 10 mM malate. Plates were inoculated with culture in the mid-log phase of growth (optical density at 600 nm [OD_{600}], 0.4 to 0.6) and grown at 28°C. Chemotactic rings were measured after 48 h of incubation. The temporal gradient assays for aerotaxis and computerized motion analysis were performed as previously described (24). Briefly, free-swimming cells were incubated on a slide placed inside a microchamber with an atmosphere of nitrogen gas (anaerobiosis) or air, which represents an attractant signal for the cells. Videos (10 s in length) for each time point were recorded, and swimming speed was analyzed through these videos using CellTrack software. The swimming speed of free-swimming cells was determined from a minimum of 75 cells tracked in 3 independent experiments. The swimming speeds denote averages calculated from the tracks of free-swimming cells 1 min prior to and 1 min after a switch from an atmosphere of N_2 to air.

Mutant construction. To generate a *cheA1* gene in which the sequence corresponding to the N-terminal TMX domain was deleted, CheA1ΔTMX, the full-length CheA1 with its putative promoter region, was amplified by PCR from genomic DNA using the CheOp-HindIII-F and CheOp-BamHI-Rev primers (Table 2). These primers include HindIII and BamHI restriction sites at their 5′ and 3′ termini, respectively, to facilitate cloning. The PCR fragment was digested with HindIII and BamHI and cloned into the pBSKII(+) vector digested with the same enzymes, yielding pBSKCheA1. An in-frame deletion of the TMX domain was obtained using pBSKCheA1 as a template in an inverse PCR strategy as described previously (44). The outward-facing primers used were CheA1ΔTMX-F2 and CheA1ΔTMX-Rev. These primers also included BglII restriction sites at their 5′ ends to facilitate recircularization after inverse PCR, generating pBSKCheA1ΔTMX. These primers allowed for an in-frame deletion of the TMX region from

TABLE 2 Primers used in this study

Primer name	Sequence[a]
CheOp-HindIII-F	5′-CCC*AAGCTT*CAGCGCGATGAACTGGTTGGACC
CheOp-BamHI-Rev	5′-CGC*GGATCC*CGTAATCAGACGGTCCTGGTTAG
CheA1ΔTMX-F2	5′-GA*AGATCT*GCGGTCGCGCGGAATTC
CheA1ΔTMX-Rev	5′-GA*AGATCT*GACCGCGTCCGCCGCACG
CheA1promXhoI-F	5′-CCG*CTCGAG*CAGCGCGATGAACTGGTT
CheA1DNup HindIII-R	5′-*AAGCTT*CACGGCGGTGACGTC
Sp245cheA1-F	5′-GAATCACGTGACGTCGGA
Sp245cheA1-R	5′-CGACGCCGCGGCCCGACA
CheA1prom KpnI-F	5′-CGG*GGTACC*CAGCGCGATGAACTGGTTG
CheA1ΔREC XhoI-R	5′-*CTCGAG*TCATGGAGCGCCCTCTCC
GWCheA1-F	5′-GGGGACAAGTTTGTACAAAAAAGCAGGCTCAGCGCGATGAACTGGTT
GWCheA1-R	5′-GGGGACCACTTTGTACAAGAAAGCTGGGTTGCGGCACCTTTCTGCTCG
GWCheA1TMX-R	5′-GGGGACCACTTTGTACAAGAAAGCTGGGTTTCCACGTCGAGCAACGAC
Tlp1GWFwd	5′-GGGGACAAGTTTGTACAAAAAGCAGGCTCCGGCATGCGGATCAGGGC
Tlp1GWRev	5′-GGGGACCACTTTGTACAAGAAAGCTGGGTCCGGCCAGCCCACCGGGCGCCT

[a]Italics indicate restriction enzyme sequences.

nucleotide 66 to 215 of the *cheA1* sequence (GenBank accession number AAL47021.1). The *cheA1*^{D1055N} mutant was generated using the QuikChange II site-directed mutagenesis kit (Stratagene), verified by sequencing, and then cloned into pCR 2.1 TOPO vector (Invitrogen). The putative *cheA1* promoter was isolated from a plasmid containing full-length *cheA1* using CheA1promXhoI-F and CheA1DNup HindIII-R, which amplify a region upstream of the *cheA1* start codon. The promoter was then cloned into the pCR2.1 TOPO vector and sequenced for verification. The *cheA1*^{D1055N} mutant and the *cheA1* promoter were then isolated by using restriction enzymes (HindIII and XbaI for isolating the *cheA1*^{D1055N} fragment and XhoI and HindIII for isolating the *cheA1* promoter) and ligated into the pBBR1MCS3 cloning vector (45). The pBBRCheA1^{D1055N} plasmid was then transformed into chemically competent *E. coli* S17-1 cells, followed by biparental conjugation into the *A. brasilense* Δ*cheA1* mutant background, as described previously (46). An *A. brasilense* strain Sp245 mutant derivative in which *cheA1* is inactivated was constructed as following. First, a 509-bp internal segment within the *cheA1* from *A. brasilense* strain Sp245, *cheA1*$_{Sp245}$, was amplified using Sp245cheA1-F and Sp245cheA1-R and then cloned into pCR 2.1 TOPO, sequenced for verification, cloned into the suicide vector pKGmob-cheA1 (Table 1), and introduced into *E. coli* chemically competent S17-1 cells (47, 48). Biparental mating was used to introduce the suicide vector carrying the internal *cheA1*$_{Sp245}$ fragment into the wild-type Sp245 strain, as described above. Single recombination mutation events were selected and verified by PCR, and a representative was used as an *A. brasilense* Sp245 Δ*cheA1*$_{Sp245}$ mutant derivative. To generate Δ*cheA1*(pBBRCheA1ΔREC), pBBRCheA1 was used as a template with the primers CheA1prom KpnI-F and CheA1ΔREC XhoI-R (Tables 1 and 2). The insert generated by PCR was digested with KpnI and XhoI, cloned into pBBR1MCS3, and digested with the same restriction enzymes. This vector was then transformed into *E. coli* S17-1 chemically competent cells and mated into the *A. brasilense* Δ*cheA1* derivative via biparental mating as described above.

Fluorescence tagging of CheA1 and its variants. Gateway cloning (Invitrogen) and the pRH005 vector were used to construct all yellow fluorescent protein (YFP) fusions (49). The pRH005 vector allows cloning of any gene to generate products fused in frame with YFP at their C termini. All genes to be fused in frame with the YFP gene in pRH005 (*cheA1*, *cheA1ΔTMX*, *tmX*, and *tlp1*) were amplified by PCR using pBBRCheA1 or pBBRCheA1ΔTMX (*cheA1*, *cheA1ΔTMX*, and *tmX*) or Sp7 genomic DNA (*tlp1*) as a template along with the following primers: for amplification of *cheA1*, GWCheA1-F and GWCheA1-R; for amplification of *cheA1ΔTMX*, GWCheA1-F and GWCheA1-R; for amplification of *tmX*, GWCheA1-F and GWCheA1TMX-R; and for amplification of *tlp1*, Tlp1GWFwd and Tlp1GWRev (Table 2). The PCR products, flanked by gateway sites on 5′ and 3′ ends, were then introduced into pDONR221 (Invitrogen), via a BP Clonase reaction (Invitrogen) and transformed into *E. coli* OmniMax chemically competent cells following the manufacturer's recommendations (Invitrogen). The constructs were verified by sequencing prior to transfer into the pRH005 vector via an LR Clonase reaction, performed per the manufacturer's instructions (Invitrogen). Final constructs were introduced into wild-type *A. brasilense* strain Sp7 and Δ*cheA1* mutant backgrounds via biparental conjugation, as described above.

Fluorescence Imaging. All cells expressing fluorescently tagged proteins were prepared by growing them to low density (OD_{600} of 0.2 to 0.4) in 5 ml of MMAB supplemented with 10 mM malate. Cells from these cultures were then pelleted via centrifugation. Thirty microliters of concentrated cells was pipetted onto a 1% low-melting-point (LMP) agarose pad in 1× phosphate-buffered saline (PBS) with a coverslip and left undisturbed for 2 to 3 min. Images were acquired using the YFP or fluorescein isothiocyanate (FITC) filter on a Nikon ECLIPSE 80i fluorescence microscope with a Nikon CoolSnap HQ2-cooled charge-coupled device (CCD) camera.

Cell length measurements. Cells to be analyzed were grown at 28°C to mid-log phase (OD_{600} of 0.4 to 0.6) in 5 ml of liquid MMAB supplemented with 18.5 mM ammonium chloride, 5 mM malate, and 5 mM fructose (17). Cells were concentrated by centrifugation, stained with 1 μM FM4-64 vital fluorescent dye (Invitrogen Molecular Probes), incubated for 5 min in the dark, centrifuged at maximum speed for 1 to 2 min, and pipetted on top of 1% LMP agarose prepared in 1× PBS. Images were acquired using the

tetramethyl rhodamine isocyanate (TRITC) filter on a Nikon ECLIPSE 80i fluorescence microscope with a Nikon CoolSnap HQ2-cooled CCD camera. Cell length measurements in micrometers were obtained using the Nikon NIS-Elements BR program from at least 50 cells per sample in four different fields of view.

Doubling time. Cells were grown at 28°C to mid-log phase (OD_{600} of 0.4 to 0.6) either in 5 ml of liquid MMAB supplemented with 18.5 mM ammonium chloride and 10 mM malate and with tetracycline (10 μg/ml) or in 5 ml of liquid TY with the same supplements. Forty microliters of the liquid culture was inoculated into 260 μl of fresh MMAB with tetracycline (10 μg/ml), and the resulting cultures underwent a growth curve on a microplate reader. The absorbance (OD_{600}) of each sample was taken every 20 min for a total of 16 h, and the doubling time was calculated from the growth curve. All curves were determined in triplicate.

Cell fractionation. Cultures were collected at log phase (OD_{600} of 0.4 to 0.6) via centrifugation at 10,000 $\times$ *g* for 10 min at 4°C, and the pellets were resuspended in 50 mM potassium phosphate buffer containing 2 mM $MgCl_2$ and 1 mM proteinase inhibitor phenylmethylsulfonyl fluoride (PMSF) (pH 7.0). Cells were then disrupted by passage through a French press three times at a cell pressure of 25,000 lb/in^2. The cell lysate was centrifuged (Fiberlite F13-14 $\times$ 50cy fixed angle rotor) at 10,000 $\times$ *g* for 20 min at 4°C, and the supernatant centrifuged at 110,000 $\times$ *g* for 120 min at 4°C (Ti 50.2 fixed-angle ultracentrifuge rotor). The pellet was suspended in the phosphate buffer once more and centrifuged again at 110,000 $\times$ *g* for 120 min at 4°C. The membrane pellet was solubilized in 1$\times$ PBS with 2% Triton X-100 and 1 mM PMSF. Protein concentrations were measured for each sample using the Bradford assay (50), and each sample was adjusted to the same protein concentration prior to loading into the SDS-polyacrylamide gel. Cell fractions were verified as membrane or cytosolic by differential staining with the hydrophobic molecular dye FM1-43, which is a lipophilic dye that fluoresces exclusively upon insertion into the cell membrane (Invitrogen Molecular Probes). The cell fractionated samples were mixed in a 1:1 ratio with the membrane-specific FM1-43 molecular dye (Invitrogen), incubated at room temperature for 15 min in the dark, and imaged by fluorescence microscopy using an FITC filter. Fluorescence intensity was compared between samples and with buffer controls exposed under similar conditions.

Western blotting. For constructs containing the pBBR1MCS3 cloning vector, 50 ml of each sample were grown to mid-log phase (OD_{600} of 0.7 to 0.8) in liquid MMAB supplemented with 18.5 mM ammonium chloride, 10 mM malate, and tetracycline (10 μg/ml). Cells were pelleted and resuspended in 200 μl fresh radioimmunoprecipitation assay (RIPA) buffer. The cells were sonicated (Fisher Sonic Dismembrator model 100) for 30 s at a 3% amplitude of pulse, followed by a 1-min rest period, for a total of five cycles. Equal volumes of protein (15 μg) and 2$\times$ Laemmli buffer with reducing agent were placed on the heat block at 70°C for 8 min and loaded into the wells of a 7.5% Mini-Protean precast gel (Bio-Rad). The gel ran at 120 V for 90 min or until the dye front reached the reference line. The gel was then transferred to a 0.45-μm hydrophobic polyvinylidene difluoride (PVDF) transfer membrane (Immobilon) using a semidry transfer apparatus (Bio-Rad). The transfer ran at 15 V for 35 min, and then the membrane was air dried for 45 min. The membrane was washed in 1$\times$ Tris-buffered saline–Tween 20 (TBST) for 5 min at room temperature before being blocked for 1.5 h at room temperature in a 5% milk solution in 1$\times$ TBST. Afterwards, the membrane was rinsed for 5 min in 1$\times$ TBST. For detection of CheA1 and variants, an anti-CheA1ΔTMX polyclonal antibody was purified using a negative-affinity protocol. Briefly, 25 ml of Δ*cheA1* cells was grown to mid-log phase and spun down. The pellet was resuspended in 0.1 M $NaHCO_3$ buffer (pH 8.3) supplemented with 0.5 M NaCl. Cells were then disrupted by passage through a French press three times at a cell pressure of 25,000 lb/in^2 and were centrifuged before the supernatant was collected. The whole-cell proteins were then immobilized onto activated Sepharose 4B beads during an overnight incubation of proteins and beads at 4°C. Unreacted proteins were washed with coupling buffer (0.1 M carbonate buffer, 0.5 M NaCl, pH 8.3), and unreacted groups were blocked by incubating the beads overnight at 4°C in 0.2 M glycine (pH 8.0). The beads were washed with coupling buffer, resuspended in 1$\times$ PBS, and loaded into a column. The column was equilibrated with 1$\times$ PBS before antiserum was passed through the column and collected. The flowthrough was reapplied to the column three times to remove any contaminants and to concentrate the antibody. We further purified this flowthrough by preparing a column containing immobilized whole proteins extracted from the Δ*che1* mutant, which lacked the entire *A. brasilense* Che1 operon (17), and passed the antiserum through the column. The resulting antibody was used at a 1:100 dilution, and a secondary antibody (Li-Cor donkey anti-rabbit IRDye 800CW) was applied at a 1:5,000 dilution for 1 h. Membranes were imaged on an Odyssey CLx infrared imaging system, and band intensities were quantified using ImageStudioLite software (4.0; Li-Cor). A minimum of four images from independent samples was used. For cell fractionated samples, a total volume of 100 ml of cells was grown to mid-log phase (OD_{600} of 0.7 to 0.8) in liquid MMAB supplemented with 18.5 mM ammonium chloride and 10 mM malate before being fractionated as described above. Equal volumes of the membrane pellet, which was resuspended in 1$\times$ PBS with 2% Triton X-100, 1 mM PMSF, and 2$\times$ Laemmli buffer with reducing agent, were boiled for 5 min prior to being loaded, at an amount of 31 μg, into an 8 to 16% Mini-Protean precast gradient gel (Bio-Rad). The gel was run at 200 V for 30 min before being transferred to a 0.2 μM nitrocellulose membrane using a semidry transfer apparatus (Bio-Rad). The transfer was performed at 15 V for 25 min, followed by membrane washes in 1$\times$ TBST for 5 min at room temperature. The membrane was blocked for 1 h at room temperature in a 5% milk solution in 1$\times$ TBST and rinsed for 5 min in 1$\times$ TBST. For the cytosolic fraction, the same protocol was followed except that the samples were loaded at a concentration of 20.5 μg and run on a 10% Mini-Protean precast gel (Bio-Rad). For detection of CheA1 in the cell fractionated samples, an anti-CheA1ΔTMX polyclonal antibody, raised against soluble CheA1ΔTMX from *A. brasilense* strain Sp7 but not further purified against whole proteins extracted from the Δ*che1*

mutant, was used at a 1:4 dilution, and a secondary antibody (Li-Cor donkey anti-rabbit IRDye 800CW) was applied at a 1:10,000 dilution for 1 h. Membranes were imaged on an Odyssey CLx Infrared imaging system. For whole-cell extracts, the same protocol as for cells bearing the pBBR1MCS3 cloning vector was used. Cells were grown as described above, and then 15 μg was loaded into the wells of a 7.5% gel Mini-Protean precast gel (Bio-Rad) and run at 120 V for 90 min or until the dye front reached the reference line. The gel was then transferred to a 0.45-μm hydrophobic PVDF transfer membrane (Immobilon) using a semidry transfer apparatus (Bio-Rad). The transfer to the nitrocellulose membrane was performed at 15 V for 35 min, and the membrane was air dried for 45 min and then washed in 1× TBST for 5 min at room temperature. The membrane was blocked for 1 h at room temperature in a 5% milk solution in 1× TBST and rinsed for 5 min in 1× TBST. The same anti-CheA1ΔTMX polyclonal antibody, which was further affinity purified with immobilized whole protein extracts from the Δ*che1* strain (17) as described above, was used at a 1:100 dilution, and the secondary antibody (Li-Cor donkey anti-rabbit IRDye 800CW) was applied for 1 h at room temperature at a 1:5,000 dilution. Samples were imaged using an Odyssey CLx infrared imaging system, and band intensities were quantified using ImageStudioLite software.

SUPPLEMENTAL MATERIAL

Supplemental material for this article may be found at https://doi.org/10.1128/JB.00189-17.

SUPPLEMENTAL FILE 1, PDF file, 0.1 MB.

ACKNOWLEDGMENTS

This work was supported by National Science Foundation (NSF) grants MCB-0919819 and MCB 1330344, awarded to G.A. We acknowledge support from the University of Tennessee College of Arts and Sciences and the BCMB department to attend the ASM Scientific Writing and Publishing Institute, which provided assistance with scientific writing development.

Any opinions, findings, conclusions, or recommendations expressed in this material are those of the authors and do not necessarily reflect the views of the National Science Foundation.

We thank Anastasia Aksenova for valuable input and technical assistance.

We declare no conflict of interest.

REFERENCES

1. Krell T, Lacal J, Munoz-Martinez F, Reyes-Darias JA, Cadirci BH, Garcia-Fontana C, Ramos JL. 2011. Diversity at its best: bacterial taxis. Environ Microbiol 13:1115–1124. https://doi.org/10.1111/j.1462-2920.2010.02383.x.
2. Alexandre G. 2010. Coupling metabolism and chemotaxis-dependent behaviours by energy taxis receptors. Microbiology 156:2283–2293. https://doi.org/10.1099/mic.0.039214-0.
3. Wadhams GH, Armitage JP. 2004. Making sense of it all: bacterial chemotaxis. Nat Rev Mol Cell Biol 5:1024–1037. https://doi.org/10.1038/nrm1524.
4. Levit MN, Stock JB. 2002. Receptor methylation controls the magnitude of stimulus-response coupling in bacterial chemotaxis. J Biol Chem 277:36760–36765. https://doi.org/10.1074/jbc.M204325200.
5. Surette MG, Levit M, Liu Y, Lukat G, Ninfa EG, Ninfa A, Stock JB. 1996. Dimerization is required for the activity of the protein histidine kinase CheA that mediates signal transduction in bacterial chemotaxis. J Biol Chem 271:939–945. https://doi.org/10.1074/jbc.271.2.939.
6. Bilwes AM, Alex LA, Crane BR, Simon MI. 1999. Structure of CheA, a signal-transducing histidine kinase. Cell 96:131–141. https://doi.org/10.1016/S0092-8674(00)80966-6.
7. Briegel A, Ladinsky MS, Oikonomou C, Jones CW, Harris MJ, Fowler DJ, Chang YW, Thompson LK, Armitage JP, Jensen GJ. 2014. Structure of bacterial cytoplasmic chemoreceptor arrays and implications for chemotactic signaling. eLife 3:e02151.
8. Briegel A, Li X, Bilwes AM, Hughes KT, Jensen GJ, Crane BR. 2012. Bacterial chemoreceptor arrays are hexagonally packed trimers of receptor dimers networked by rings of kinase and coupling proteins. Proc Natl Acad Sci U S A 109:3766–3771. https://doi.org/10.1073/pnas.1115719109.
9. Li M, Hazelbauer GL. 2011. Core unit of chemotaxis signaling complexes. Proc Natl Acad Sci U S A 108:9390–9395. https://doi.org/10.1073/pnas.1104824108.
10. Sun H, Zusman DR, Shi W. 2000. Type IV pilus of *Myxococcus xanthus* is a motility apparatus controlled by the frz chemosensory system. Curr Biol 10:1143–1146. https://doi.org/10.1016/S0960-9822(00)00705-3.
11. Güvener ZT, Harwood CS. 2007. Subcellular location characteristics of the *Pseudomonas aeruginosa* GGDEF protein, WspR, indicate that it produces cyclic-di-GMP in response to growth on surfaces. Mol Microbiol 66:1459–1473.
12. Kirby JR, Zusman DR. 2003. Chemosensory regulation of developmental gene expression in *Myxococcus xanthus*. Proc Natl Acad Sci U S A 100:2008–2013. https://doi.org/10.1073/pnas.0330944100.
13. Bible AN, Khalsa-Moyers GK, Mukherjee T, Green CS, Mishra P, Purcell A, Aksenova A, Hurst GB, Alexandre G. 2015. Metabolic adaptations of *Azospirillum brasilense* to oxygen stress by cell-to-cell clumping and flocculation. Appl Environ Microbiol 81:8346–8357. https://doi.org/10.1128/AEM.02782-15.
14. Berleman JE, Bauer CE. 2005. Involvement of a Che-like signal transduction cascade in regulating cyst cell development in *Rhodospirillum centenum*. Mol Microbiol 56:1457–1466. https://doi.org/10.1111/j.1365-2958.2005.04646.x.
15. Wuichet K, Zhulin IB. 2010. Origins and diversification of a complex signal transduction system in prokaryotes. Sci Signal 3:ra50. https://doi.org/10.1126/scisignal.2000724.
16. Bible A, Russell MH, Alexandre G. 2012. The *Azospirillum brasilense* Che1 chemotaxis pathway controls swimming velocity, which affects transient cell-to-cell clumping. J Bacteriol 194:3343–3355. https://doi.org/10.1128/JB.00310-12.
17. Bible AN, Stephens BB, Ortega DR, Xie Z, Alexandre G. 2008. Function of a chemotaxis-like signal transduction pathway in modulating motility, cell clumping, and cell length in the alphaproteobacterium *Azospirillum brasilense*. J Bacteriol 190:6365–6375. https://doi.org/10.1128/JB.00734-08.
18. Qi X, Nellas RB, Byrn MW, Russell MH, Bible AN, Alexandre G, Shen T. 2013. Swimming motility plays a key role in the stochastic dynamics of

cell clumping. Phys Biol 10:026005. https://doi.org/10.1088/1478-3975/10/2/026005.
19. Mukherjee T, Kumar D, Burriss N, Xie Z, Alexandre G. 27 May 2016. *Azospirillum brasilense* chemotaxis depends on two signaling pathways regulating distinct motility parameters. J Bacteriol https://doi.org/10.1128/jb.00020-16.
20. Hauwaerts D, Alexandre G, Das SK, Vanderleyden J, Zhulin IB. 2002. A major chemotaxis gene cluster in *Azospirillum brasilense* and relationships between chemotaxis operons in α-proteobacteria. FEMS Microbiol Lett 208:61–67.
21. Ponting CP, Schultz J, Milpetz F, Bork P. 1999. SMART: identification and annotation of domains from signalling and extracellular protein sequences. Nucleic Acids Res 27:229–232. https://doi.org/10.1093/nar/27.1.229.
22. Kentner D, Sourjik V. 2006. Spatial organization of the bacterial chemotaxis system. Curr Opin Microbiol 9:619–624. https://doi.org/10.1016/j.mib.2006.10.012.
23. Greer-Phillips SE, Stephens BB, Alexandre G. 2004. An energy taxis transducer promotes root colonization by *Azospirillum brasilense*. J Bacteriol 186:6595–6604. https://doi.org/10.1128/JB.186.19.6595-6604.2004.
24. Russell MH, Bible AN, Fang X, Gooding JR, Campagna SR, Gomelsky M, Alexandre G. 2013. Integration of the second messenger c-di-GMP into the chemotactic signaling pathway. mBio 4:e00001-13. https://doi.org/10.1128/mBio.00001-13.
25. Xie Z, Ulrich LE, Zhulin IB, Alexandre G. 2010. PAS domain containing chemoreceptor couples dynamic changes in metabolism with chemotaxis. Proc Natl Acad Sci U A 107:2235–2240. https://doi.org/10.1073/pnas.0910055107.
26. Baida GE, Kuzmin NP. 1995. Cloning and primary structure of a new hemolysin gene from *Bacillus cereus*. Biochim Biophys Acta 1264:151–154. https://doi.org/10.1016/0167-4781(95)00150-F.
27. Finn RD, Bateman A, Clements J, Coggill P, Eberhardt RY, Eddy SR, Heger A, Hetherington K, Holm L, Mistry J, Sonnhammer ELL, Tate J, Punta M. 2014. Pfam: the protein families database. Nucleic Acids Res 42:D222–D230. https://doi.org/10.1093/nar/gkt1223.
28. Chen Y-C, Chang M-C, Chuang Y-C, Jeang C-L. 2004. Characterization and virulence of hemolysin III from *Vibrio vulnificus*. Curr Microbiol 49:175–179. https://doi.org/10.1007/s00284-004-4288-5.
29. Tang YT, Hu T, Arterburn M, Boyle B, Bright JM, Emtage PC, Funk WD. 2005. PAQR proteins: a novel membrane receptor family defined by an ancient 7-transmembrane pass motif. J Mol Evol 61:372–380. https://doi.org/10.1007/s00239-004-0375-2.
30. Inclan YF, Laurent S, Zusman DR. 2008. The receiver domain of FrzE, a CheA-CheY fusion protein, regulates the CheA histidine kinase activity and downstream signalling to the A- and S-motility systems of *Myxococcus xanthus*. Mol Microbiol 68:1328–1339. https://doi.org/10.1111/j.1365-2958.2008.06238.x.
31. He K, Marden JN, Quardokus EM, Bauer CE. 2013. Phosphate flow between hybrid histidine kinases CheA(3) and CheS(3) controls *Rhodospirillum centenum* cyst formation. PLoS Genet 9:e1004002. https://doi.org/10.1371/journal.pgen.1004002.
32. Kofoid EC, Parkinson JS. 1991. Tandem translation starts in the *cheA* locus of *Escherichia coli*. J Bacteriol 173:2116–2119. https://doi.org/10.1128/jb.173.6.2116-2119.1991.
33. Smith RA, Parkinson JS. 1980. Overlapping genes at the *cheA* locus of *Escherichia coli*. Proc Natl Acad Sci U S A 77:5370–5374. https://doi.org/10.1073/pnas.77.9.5370.
34. Wisniewski-Dyé F, Borziak K, Khalsa-Moyers G, Alexandre G, Sukharnikov LO, Wuichet K, Hurst GB, McDonald WH, Robertson JS, Barbe V, Calteau A, Rouy Z, Mangenot S, Prigent-Combaret C, Normand P, Boyer M, Siguier P, Dessaux Y, Elmerich C, Condemine G, Krishnen G, Kennedy I, Paterson AH, González V, Mavingui P, Zhulin IB. 2011. *Azospirillum* genomes reveal transition of bacteria from aquatic to terrestrial environments. PLoS Genet 7:e1002430. https://doi.org/10.1371/journal.pgen.1002430.
35. Kaneko T, Minamisawa K, Isawa T, Nakatsukasa H, Mitsui H, Kawaharada Y, Nakamura Y, Watanabe A, Kawashima K, Ono A, Shimizu Y, Takahashi C, Minami C, Fujishiro T, Kohara M, Katoh M, Nakazaki N, Nakayama S, Yamada M, Tabata S, Sato S. 2010. Complete genomic structure of the cultivated rice endophyte *Azospirillum* sp. B510. DNA Res 17:37–50. https://doi.org/10.1093/dnares/dsp026.
36. Rivera D, Revale S, Molina R, Gualpa J, Puente M, Maroniche G, Paris G, Baker D, Clavijo B, McLay K, Spaepen S, Perticari A, Vazquez M, Wisniewski-Dyé F, Watkins C, Martinez-Abarca F, Vanderleyden J, Cassan F. 2014. Complete genome sequence of the model rhizosphere strain *Azospirillum brasilense* Az39, successfully applied in agriculture. Genome Announc 2:e00683-14. https://doi.org/10.1128/genomeA.00683-14.
37. Kwak Y, Shin JH. 2015. First *Azospirillum* genome from aquatic environments: whole-genome sequence of *Azospirillum thiophilum* BV-S, a novel diazotroph harboring a capacity of sulfur-chemolithotrophy from a sulfide spring. Mar Genomics https://doi.org/10.1016/j.margen.2015.11.001.
38. Wisniewski-Dyé F, Lozano L, Acosta-Cruz E, Borland S, Drogue B, Prigent-Combaret C, Rouy Z, Barbe V, Herrera AM, Gonzalez V, Mavingui P. 2012. Genome sequence of *Azospirillum brasilense* CBG497 and comparative analyses of *Azospirillum* core and accessory genomes provide insight into niche adaptation. Genes (Basel) 3:576–602.
39. Martin-Didonet CC, Chubatsu LS, Souza EM, Kleina M, Rego FG, Rigo LU, Yates MG, Pedrosa FO. 2000. Genome structure of the genus *Azospirillum*. J Bacteriol 182:4113–4116. https://doi.org/10.1128/JB.182.14.4113-4116.2000.
40. Pasek S, Risler JL, Brezellec P. 2006. Gene fusion/fission is a major contributor to evolution of multi-domain bacterial proteins. Bioinformatics 22:1418–1423. https://doi.org/10.1093/bioinformatics/btl135.
41. Marcotte EM, Pellegrini M, Ng HL, Rice DW, Yeates TO, Eisenberg D. 1999. Detecting protein function and protein-protein interactions from genome sequences. Science 285:751–753. https://doi.org/10.1126/science.285.5428.751.
42. Baldani VLD, de B Alvarez MA, Baldani JI, xd, Bereiner J. 1986. Establishment of inoculated *Azospirillum* spp. in the rhizosphere and in roots of field grown wheat and sorghum. Plant Soil 90:35–46. https://doi.org/10.1007/BF02277385.
43. Vanstockem M, Michiels K, Vanderleyden J, Van Gool AP. 1987. Transposon mutagenesis of *Azospirillum brasilense* and *Azospirillum lipoferum*: physical analysis of Tn5 and Tn5-Mob insertion mutants. Appl Environ Microbiol 53:410–415.
44. Tomic-Canic M, Bernerd F, Blumenberg M. 1996. A simple method to introduce internal deletions or mutations into any position of a target DNA sequence. Methods Mol Biol 57:249–257.
45. Kovach ME, Elzer PH, Hill DS, Robertson GT, Farris MA, Roop RM, II, Peterson KM. 1995. Four new derivatives of the broad-host-range cloning vector pBBR1MCS, carrying different antibiotic-resistance cassettes. Gene 166:175–176. https://doi.org/10.1016/0378-1119(95)00584-1.
46. Stephens BB, Loar SN, Alexandre G. 2006. Role of CheB and CheR in the complex chemotactic and aerotactic pathway of *Azospirillum brasilense*. J Bacteriol 188:4759–4768. https://doi.org/10.1128/JB.00267-06.
47. Simon R, Priefer U, Puhler A. 1983. A broad host range mobilization system for in vivo genetic engineering: transposon mutagenesis in gram negative bacteria. Nat Biotechnol 1:784–791. https://doi.org/10.1038/nbt1183-784.
48. Katzen F, Becker A, Ielmini MV, Oddo CG, Ielpi L. 1999. New mobilizable vectors suitable for gene replacement in gram-negative bacteria and their use in mapping of the 3′ end of the *Xanthomonas campestris* pv. *campestris gum* operon Appl Environ Microbiol 65:278–282.
49. Hallez R, Letesson JJ, Vandenhaute J, De Bolle X. 2007. Gateway-based destination vectors for functional analyses of bacterial ORFeomes: application to the Min system in *Brucella abortus*. Appl Environ Microbiol 73:1375–1379. https://doi.org/10.1128/AEM.01873-06.
50. Bradford MM. 1976. A rapid and sensitive method for the quantitation of microgram quantities of protein utilizing the principle of protein-dye binding. Anal Biochem 72:248–254. https://doi.org/10.1016/0003-2697(76)90527-3.